

PAPER

Multimodal contrastive learning for spatial gene expression prediction using histology images

Wenwen Min¹, Zhiceng Shi¹, Jun Zhang¹, Jun Wan² and Changmiao Wang³¹School of Information Science and Engineering, Yunnan University, 650091, Kunming, China, ²School of Information and Safety Engineering, Zhongnan University of Economics and Law, 430073, Wuhan, China and ³Shenzhen Research Institute of Big Data, 518172, Shenzhen, China*Corresponding author: minwenwen@ynu.edu.cn

FOR PUBLISHER ONLY Received on Date Month Year; revised on Date Month Year; accepted on Date Month Year

Abstract

In recent years, the advent of spatial transcriptomics (ST) technology has unlocked unprecedented opportunities for delving into the complexities of gene expression patterns within intricate biological systems. Despite its transformative potential, the prohibitive cost of ST technology remains a significant barrier to its widespread adoption in large-scale studies. An alternative, more cost-effective strategy involves employing artificial intelligence to predict gene expression levels using readily accessible whole-slide images (WSIs) stained with Hematoxylin and Eosin (H&E). However, existing methods have yet to fully capitalize on multimodal information provided by H&E images and ST data with spatial location. In this paper, we propose **mclSTExp**, a multimodal contrastive learning with Transformer and Densenet-121 encoder for Spatial Transcriptomics Expression prediction. We conceptualize each spot as a "word", integrating its intrinsic features with spatial context through the self-attention mechanism of a Transformer encoder. This integration is further enriched by incorporating image features via contrastive learning, thereby enhancing the predictive capability of our model. Our extensive evaluation of **mclSTExp** on two breast cancer datasets and a skin squamous cell carcinoma dataset demonstrates its superior performance in predicting spatial gene expression. Moreover, **mclSTExp** has shown promise in interpreting cancer-specific overexpressed genes, elucidating immune-related genes, and identifying specialized spatial domains annotated by pathologists. Our source code is available at <https://github.com/shizhiceng/mclSTExp>.

Key words: Spatial Transcriptomics, Histology Images, Multimodal Contrastive Learning, Transformer Encoder

Introduction

With the rapid development of ST technology, we may gain a more comprehensive understanding of gene expression patterns within complex biological systems [1]. Compared to traditional transcriptomics, this technology enables high-throughput RNA sequencing across entire tissue sections while preserving spatial information regarding cell locations within tissue slices, allowing researchers to visually observe the spatial distribution of gene expression [2, 3]. The insights afforded by this technology extend beyond gene expression, offering novel perspectives on cell-cell interactions and molecular signaling pathways within the research domain [4]. Despite these advancements, effectively harnessing the unique attributes of ST data to investigate spatial gene expression patterns and develop spatial gene detection methodologies at varying resolutions remains challenging [5]. In order to fully utilize spatial location information, several novel computational methods have been developed for spatial domain recognition (SEDR [6], STAGATE [7], CCST [8], STMASK [9] etc.) and exploring super-resolution gene expression patterns

(BayesSpace [5], iStar [10], TESLA [11], etc.) and imputing ST data [12].

Despite the rapid development of ST technology, the cost of generating such data remains relatively high, thus limiting the applicability of ST technology in large-scale studies. In contrast, whole-slide images (WSIs) [13, 14, 15] stained with Hematoxylin and Eosin (H&E) are more readily available, cost-effective, and widely used in clinical practice. Using H&E images to predict ST gene expression profiles has become a more common and cost-effective research approach [16, 17]. In recent studies, Schmauch et al. confirmed the feasibility of using H&E images to predict ST gene expression profiles [18]. Their developed HE2RNA method performed excellently in capturing subtle structures within H&E images, revealing critical tumor regions specific to certain cancer types.

Pathological images (such as H&E images) reveal the cellular structure, morphological features, and pathological changes within tissues, while ST technology elucidates gene expression patterns and their spatial distribution. Integrating this information is crucial for a deeper understanding of disease pathogenesis, prognosis assessment, and the development of personalized treatment strategies [19, 20, 21]. Several methods,

such as STnet [22], HisToGene [16], His2ST [23], THItToGene [24], and Bleep [25], have been explored for integrating histopathological images with transcriptomic data. STnet segments tissue slice images into different patches and encodes each patch using DenseNet [26], which are then embedded into the feature space and projected onto the dimension of gene expression through fully connected layers. HisToGene employs a Vision Transformer (ViT) [27] to encode each patch and enhances spatial relationships between patches through a self-attention mechanism. His2ST introduces a graph neural network (GNN) [28] to better learn spatial relationships between spots, thus improving performance. THItToGene utilizes H&E images as input and employs dynamic convolutional and capsule networks to capture signals of potential molecular features within histological samples. Bleep utilizes a contrastive learning [29] approach, introducing image and gene expression encoders to learn joint embedding in space.

However, none of the aforementioned methods have effectively integrated the multimodal information provided by H&E images and ST data with spatial location. To address this issue, we propose mclSTExp, a multimodal deep learning approach utilizing Transformer and contrastive learning architecture. Inspired by the field of natural language processing, we regard the spots detected by ST technology as “words” and the sequences of these spots as “sentences” containing multiple “words”. We employ a self-attention mechanism to extract features from these “words” and combine them with learnable position encoding to seamlessly integrate the positional information of these “words”. Subsequently, we employ a contrastive learning framework to fuse the combined features with image features. Our experimental results demonstrate that mclSTExp accurately predicts gene expression in H&E images at different spatial resolutions. This is achieved by leveraging the features of each spot, its spatial information, and H&E image features. Additionally, mclSTExp demonstrates the ability to interpret specific cancer-overexpressed genes, immunologically relevant genes, preserve the original gene expression patterns, and identify specific spatial domains annotated by pathologists (Supplementary Note 1).

Materials and Methods

Dataset description

The proposed mclSTExp and competing methods are evaluated on three real datasets. The detailed description of the datasets and the preprocessing process can be found in the Supplementary Note 2 and Table S1.

Overview of mclSTExp

The proposed mclSTExp learns a multimodal embedding space from H&E images, spot gene expression data, and spot positional information (Figure 1). Specifically, the image is passed through an image encoder to capture visual features, while the spot’s gene expression data along with its positional encoding is input to the Spot encoder to capture fused features incorporating spatial information. Contrastive learning is then applied to the obtained visual features and fused features, maximizing the cosine similarity of embedding for truly paired images and gene expressions, while minimizing the similarity for incorrectly paired embedding. This facilitates the fusion of image features, thereby further enhancing the model’s representational capacity.

To predict spatial gene expression from an test image, the image is fed into the image encoder to extract its visual features. Subsequently, the cosine similarity is computed between the obtained visual features and the features of N spots (consistent with the training process). The top k spot features with the highest similarity scores are selected, and their corresponding ground truth gene expressions are weightedly aggregated to infer the gene expression of the test images.

Image and Spot encoders

We segment 224×224 pixel image patches from H&E images based on the positions of spots. For each extracted image patch Patch_i , we utilized pre-train DenseNet-121 to embed it into feature z_i^{Patch} , followed by projecting it into a feature space using a projection layer. In contrast to the skip connections in ResNet [30], the dense connectivity mechanism in DenseNet-121 enhances the reusability of features, aiding the neural network in capturing image features more effectively and thereby strengthening the model’s expressive capability [26].

$$z_i^{\text{Patch}} = \text{Densenet-121}(\text{patch}_i), \quad (1)$$

$$h_i^{\text{Patch}} = \text{MLP}(z_i^{\text{Patch}}). \quad (2)$$

Inspired by the field of natural language processing, we regard the spots detected by ST technology as “words” and the sequences of these spots as “sentences” containing multiple “words”. We employ a self-attention mechanism to extract features from these “words” and combine them with learnable position encoding to seamlessly integrate the positional information of these “words”. Multi-head attention is an extension of the attention mechanism, enhancing the model’s ability to capture complex patterns and global information in input sequences by simultaneously learning multiple independent sets of attention weights as follows:

$$\text{MHSA}(Q, K, V) = [\text{head}_1, \dots, \text{head}_n]W_0, \quad (3)$$

where W_0 represents the weight matrix used for aggregating the attention heads, while n denotes the number of heads. Additionally, Q , K , and V correspond to Query, Key, and Value, respectively. The attention mechanism is defined as follows:

$$\text{head}_i = \text{Attention}(QW_i^Q, KW_i^K, VW_i^V), \quad (4)$$

$$\text{Attention}(Q, K, V) = \text{softmax}\left(\frac{QK^T}{\sqrt{d_k}}\right)V, \quad (5)$$

where W_i^Q , W_i^K and W_i^V are weight matrices. The term $\left(\frac{QK^T}{\sqrt{d_k}}\right)$ is called Attention Map, whose shape is $N \times N$. The term V is the value of the self-attention mechanism, where $V = Q = K$.

Regarding the positional information of spots, each spot’s coordinates (x, y) are represented by a matrix of size $N \times 2$. The x -coordinate information is transformed into a one-hot encoding matrix P_x of size $N \times n$, where n is the maximum number of x -coordinates across all tissue sections. For the all datasets, $n = 65536$. Then, the matrix is linearly transformed using the learnable linear layer W_x to obtain an $N \times \text{hvg-num}$ matrix S_x that maintains the same dimensions as the Spots ($\text{Spots} \in \mathbb{R}^{\text{spot-num}, \text{hvg-num}}$). Similarly, the y -coordinate vector undergoes a similar transformation to obtain an $N \times \text{hvg-num}$ encoding matrix S_y . Finally, the spot feature, x -coordinate encoding matrix S_x , and y -coordinate encoding matrix S_y

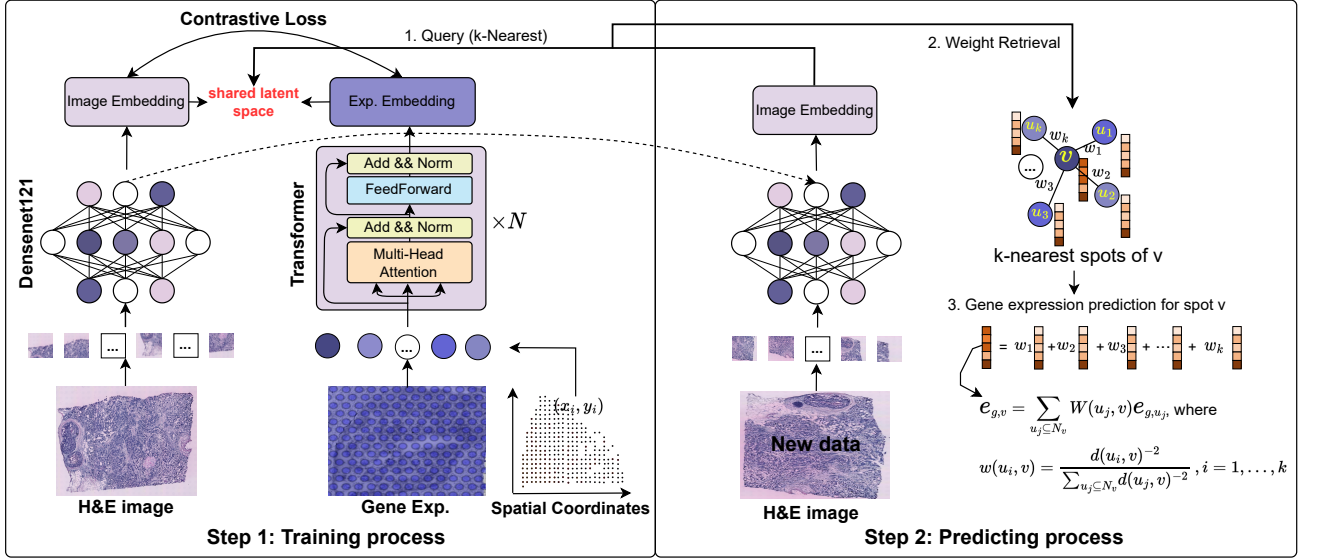


Figure 1. The architecture of the proposed mclSTExp model. Step 1: mclSTExp seamlessly integrates spot features with their positional information using the self-attention mechanism of Transformer. Subsequently, it fuses H&E image information through contrastive learning, thus learning a multimodal embedding space enriched with diverse features. Step 2: Projected image patches into the learned multimodal embedding space to query the expressions of the nearest k spots; inferred the gene expression of the test image by weighted aggregation of these queried spot expressions.

are combined and passed through a multi-head attention mechanism using Eq.(3):

$$z_i^{\text{spot}} = \text{MHSA}(\text{Spot}_i + S_x + S_y), \quad (6)$$

Then, project it into a feature space using a projection layer:

$$h_i^{\text{spot}} = \text{MLP}(z_i^{\text{spot}}). \quad (7)$$

In this feature space, the dimensions of h_i^{patch} and h_i^{spot} are both $N \times 256$.

We utilize a self-attention mechanism to integrate the gene expression features and spatial location features of spots. This multimodal feature representation not only integrates critical information from gene expression but also takes into account the specific spatial location of each point within the tissue image. As a result, each spot in the feature space exhibits a more distinct and enriched expression. Specifically, the partitioning of H&E image patches is based on the positions of spots. Therefore, spots and patches located at the same position inherently form a positive sample pair, while those at different positions constitute negative sample pairs.

Contrastive learning module

We adopt a contrastive learning approach to reduce the distance between positive sample pairs and increase the distance between negative sample pairs, thereby achieving the fusion of image information. Specifically, in each batch comprising N pairs of (patch, spot). We utilize the mclSTExp algorithm to simultaneously train both the image encoder and Spot encoder, aiming to construct a multimodal embedding space. The optimization objective of this space is to maximize the cosine similarity of N positive sample pairs and simultaneously minimize the cosine similarity of $N^2 - N$ negative sample pairs. We employ the loss function of CLIP [31] and fine-tune it to suit our task.

For integrating positive sample pairs, we employ a label matrix where diagonal elements represent positive sample pairs

(labeled as 1), and non-diagonal elements represent negative sample pairs (labeled as 0). Subsequently, we utilize the cross-entropy loss function to achieve effective classification.

To show the overall loss of our model, we first define the cosine similarity function cos_sim between patch and spot embedding as follows:

$$\text{cos_sim}(\mathbf{h}^{\text{patch}}, \mathbf{h}^{\text{spot}}) = \mathbf{h}^{\text{patch}} \cdot (\mathbf{h}^{\text{spot}})^T, \quad (8)$$

where the “label” matrix is defined as:

$$\text{label} = \begin{bmatrix} 1 & 0 & 0 & \dots \\ 0 & 1 & 0 & \dots \\ \vdots & \vdots & \ddots & \vdots \\ 0 & 0 & \dots & 1 \end{bmatrix} \quad (9)$$

And the cosine similarity function between spot and patch embedding is defined as:

$$\text{cos_sim}(\mathbf{h}^{\text{spot}}, \mathbf{h}^{\text{patch}}) = \mathbf{h}^{\text{spot}} \cdot (\mathbf{h}^{\text{patch}})^T. \quad (10)$$

Two individual loss components, $\text{loss}_{\text{image}}$ and $\text{loss}_{\text{spot}}$, are computed using the cross-entropy loss function (CE_Loss).

$$\text{Loss}_{\text{image}} = \text{CE_Loss}(\text{cos_sim}(\mathbf{h}^{\text{patch}}, \mathbf{h}^{\text{spot}}), \text{label}), \quad (11)$$

$$\text{Loss}_{\text{spot}} = \text{CE_Loss}(\text{cos_sim}(\mathbf{h}^{\text{spot}}, \mathbf{h}^{\text{patch}}), \text{label}), \quad (12)$$

where $\text{Loss}_{\text{image}}$ is based on the similarity between the image embedding and the transpose of spot embedding, while $\text{Loss}_{\text{spot}}$ is based on the similarity between spot embedding and the transpose of image embedding.

Finally, the overall loss of our model is calculated as the average of these two losses:

$$\text{Loss} = (\text{Loss}_{\text{image}} + \text{Loss}_{\text{spot}})/2. \quad (13)$$

Table 1. For the HER2+, cSCC, and Alex+10x datasets, the mean Pearson correlation coefficients (PCCs) for the predicted expression levels of All Considered Genes (ACG) and the top 50 most Highly Expressed Genes (HEG), as well as the average Mean Squared Error (MSE) and Mean Absolute Error (MAE), were calculate compared to the ground truth expressions.

Methods	HER2+			
	PCC (ACG)	PCC (HEG)	MSE	MAE
STnet [22]	0.0561 \pm 0.017	0.0134 \pm 0.013	0.5312 \pm 0.008	0.6306 \pm 0.011
HisToGene [16]	0.0842 \pm 0.015	0.0711 \pm 0.014	0.5202 \pm 0.014	0.6422 \pm 0.005
His2ST [23]	0.1443 \pm 0.013	0.1849 \pm 0.015	0.5135 \pm 0.009	0.6087 \pm 0.013
THItGene [24]	0.1726 \pm 0.018	0.2809 \pm 0.013	0.5012 \pm 0.011	0.5956 \pm 0.009
BLEEP [25]	0.1873 \pm 0.005	0.2909 \pm 0.016	0.6015 \pm 0.016	0.5824 \pm 0.004
mclSTExp (ours)	0.2304 \pm 0.011	0.3866 \pm 0.021	0.5897 \pm 0.013	0.5813 \pm 0.008
Methods	cSCC			
	PCC (ACG)	PCC (HEG)	MSE	MAE
STnet [22]	0.0012 \pm 0.022	0.0018 \pm 0.015	0.6806 \pm 0.006	0.6404 \pm 0.003
HisToGene [16]	0.0771 \pm 0.024	0.0919 \pm 0.012	0.6805 \pm 0.012	0.6234 \pm 0.007
His2ST [23]	0.1838 \pm 0.011	0.2175 \pm 0.016	0.6748 \pm 0.017	0.6107 \pm 0.006
THItGene [24]	0.2373 \pm 0.009	0.2719 \pm 0.012	0.6546 \pm 0.006	0.6012 \pm 0.019
BLEEP [25]	0.2449 \pm 0.017	0.3122 \pm 0.027	0.5163 \pm 0.007	0.5399 \pm 0.015
mclSTExp (ours)	0.3235 \pm 0.019	0.4261 \pm 0.016	0.4302 \pm 0.005	0.5208 \pm 0.009
Methods	Alex+10x			
	PCC (ACG)	PCC (HEG)	MSE	MAE
STnet [22]	0.0009 \pm 0.013	0.0452 \pm 0.007	0.4721 \pm 0.011	0.5042 \pm 0.015
HisToGene [16]	0.0618 \pm 0.008	0.0984 \pm 0.015	0.4565 \pm 0.014	0.4973 \pm 0.009
His2ST [23]	0.1299 \pm 0.012	0.1784 \pm 0.005	0.3788 \pm 0.008	0.4492 \pm 0.012
THItGene [24]	0.1384 \pm 0.014	0.2156 \pm 0.013	0.3672 \pm 0.009	0.4315 \pm 0.006
BLEEP [25]	0.1552 \pm 0.009	0.2825 \pm 0.012	0.2593 \pm 0.013	0.4050 \pm 0.015
mclSTExp (ours)	0.1949 \pm 0.011	0.3611 \pm 0.018	0.2329 \pm 0.006	0.3897 \pm 0.011

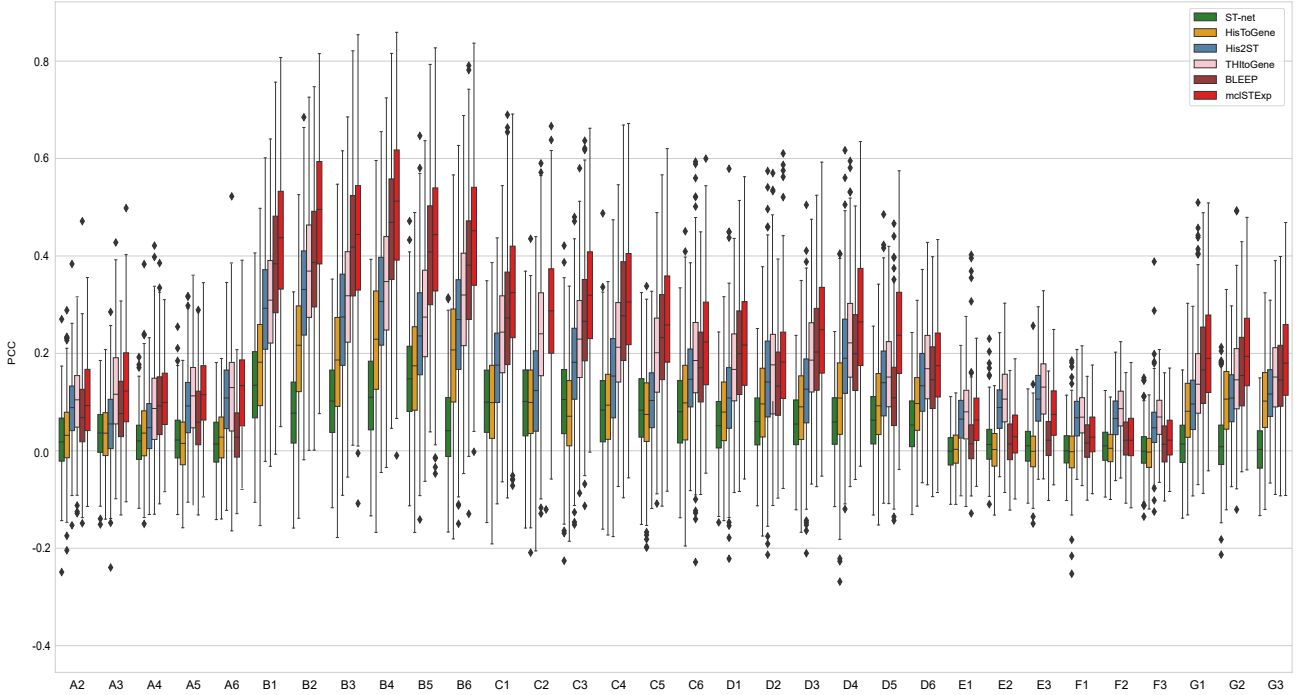


Figure 2. Evaluation of gene expression prediction on the HER2+ datasets by the PCCs between the observed and predicted gene expression by STnet [22], HisToGene [16], His2ST [23], THItGene [24], BLEEP [25] and mclSTExp.

Weight aggregation module

As illustrated in Step 2 of Figure 1, the procedure commences by segmenting the H&E image into N small patches, which are later encoded by the pre-trained image encoder. Once the image patches are represented in the joint embedding space,

the process transitions to predicting the gene expression of an image. To initiate this prediction, the test image data (new data) is input into an image encoder, extracting its visual features. Within the established shared embedding space, the cosine similarity is then computed between the

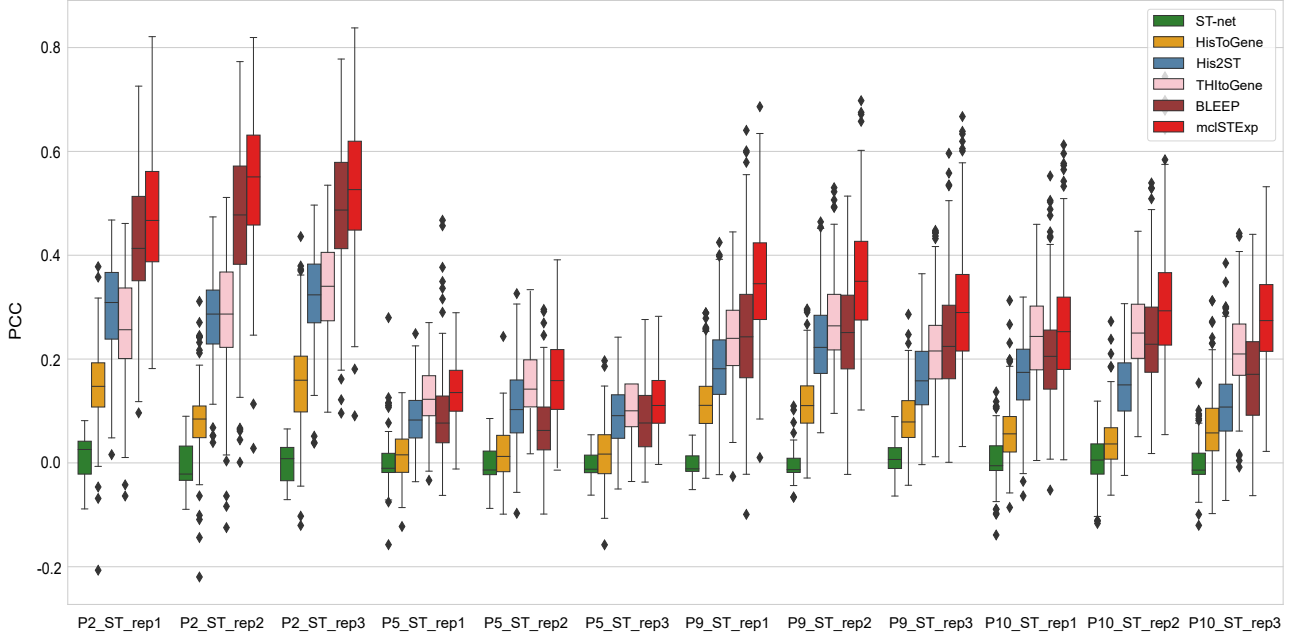


Figure 3. Evaluation of gene expression prediction on the cSCC datasets by the PCCs between the observed and predicted gene expression by STnet [22], HisToGene [16], His2ST [23], THIttoGene [24], BLEEP [25] and mclSTExp.

visual features of the test image (new data) and all spot features, maintaining consistency with the training process. Subsequently, the top k spot features with the highest similarity scores are discerned. The Euclidean distance is calculated within the shared embedding space between the visual features of the image and spot features as follows:

$$d(u, v) = \sqrt{\sum_{i=1}^n (u_i - v_i)^2}, \quad (14)$$

where n represents the dimensionality of the feature space, the next step involves inferring the gene expression value for spot v by using the weighted distance [11] of the gene expressions of the top k spots based on their similarity scores. The weights are defined as follows:

$$W(u_i, v) = \frac{d(u_i, v)^{-2}}{\sum_{u_j \in N_v} d(u_j, v)^{-2}}, \quad (15)$$

$$e_{g,v} = \sum_{u_j \in N_v} W(u_j, v) e_{g,u_j}. \quad (16)$$

where e_{g,u_j} represents the observed gene expression for spot u_j .

Results

The details on the baseline methods, experimental settings, and evaluation criteria can be found in [Supplementary Notes 3, 4 and 5](#).

mclSTExp can improve the prediction accuracy

To assess the performance of mclSTExp, we analyze the HER2+ breast cancer dataset, which includes 32 tissue sections, the cSCC dataset with 12 tissue sections, and the Alex+10x dataset with 9 slices (Table 1). For the evaluation of gene expression prediction accuracy, we conduct leave-one-out cross-validation.

Specifically, for each dataset, we used one slice as the test set and the remaining slices as the training set. For each tissue section, we computed the PCC for all considered genes (ACG) as well as the top 50 highly expressed genes (HEG), along with the MSE and MAE for all considered genes. Subsequently, the average values of PCC (ACG), PCC (HEG), MSE, and MAE across all tissue sections were calculated to evaluate the overall model performance. We compared mclSTExp with five other recently developed advanced methods for predicting spatial gene expression. Considering that the gene expression prediction task emphasizes capturing relative changes, we preferred evaluation metrics related to PCC. As shown in Table 1, mclSTExp achieved the highest average PCC for both ACG and HEG across these three datasets. Specifically, the PCC (ACG) of mclSTExp was 23.01%, 32.09%, and 25.57% higher than that of the second-ranked method BLEEP on these three datasets, while the PCC (HEG) was 32.89%, 36.48%, and 27.82% higher, respectively.

To examine the results of each slice individually, we visualized the PCC between the gene expression predicted by mclSTExp and the observed gene expression on each slice. As depicted in Figure 2, mclSTExp attained the highest PCC among the 32 slices in the HER2+ dataset, achieving this distinction on 26 slices. However, for slices E1-F3, the PCC values across all methods were relatively low, suggesting potential issues with gene detection sensitivity or specificity in ST technology. Notably, mclSTExp consistently outperformed the second-ranked method Bleep across all slices. Additionally, mclSTExp demonstrated the highest PCC across all tissue sections in the cSCC dataset, as depicted in Figure 3. Noteworthy is its substantial improvement in predicting gene expression correlation, particularly for the P10_ST_rep3 section. In Figure 4, mclSTExp exhibited the highest PCC on 7 out of 9 slices in the Alex+10x dataset. However, for slice 1142243F, the PCC scores for all methods were notably low. This lower score may be attributed to various factors,

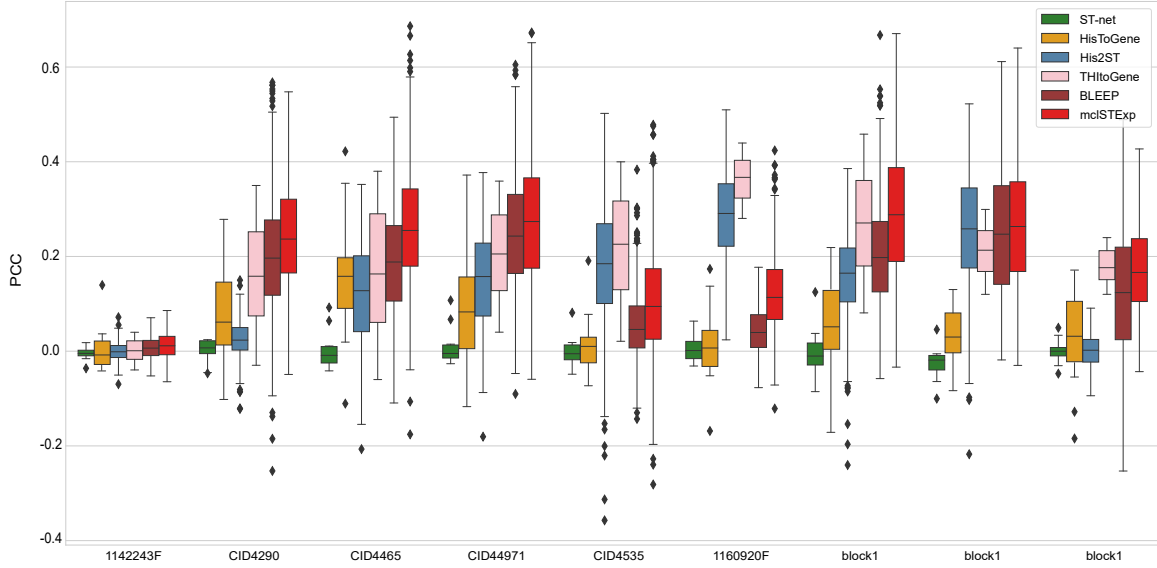


Figure 4. Evaluation of gene expression prediction on the Alex+10x datasets by the PCCs between the observed and predicted gene expression by STnet [22], HisToGene [16], His2ST [23], THItGene [24], BLEEP [25] and mclSTExp.

including a weak correlation between the expression of specific genes and morphological features, suboptimal detection of certain genes by the Visium platform leading to challenges in predicting their expression, and the potential influence of non-biological variations introduced artificially during the experiment, independent of the image itself.

Visualization of the predicted gene expression

To further evaluate the predicted gene expression, we explored whether the gene expression predicted by mclSTExp accurately reflected the actual status of tumor-related genes. Across all datasets, we analyzed the correlation between observed gene expression and predicted gene expression, calculating correlation coefficients and P-values for each spot. Subsequently, we computed the average $-\log_{10}$ (P-values) for all genes. These genes were ranked in descending order of their $-\log_{10}$ (P-values), as detailed in [Supplementary Table S2](#). For the HER2+ dataset, we visualized the top seven genes: *GANS*, *FN1*, *FASN*, *HLA-B*, *SCD*, *IGKC*, and *HLA-DRA*. As shown in Figure 5, the PCCs for these genes using mclSTExp were 0.840, 0.815, 0.780, 0.844, 0.808, 0.629, and 0.833, respectively, surpassing those predicted by the second-ranked method, Bleep, by 11.1%, 18.6%, 18.5%, 4.7%, 28.4%, 16.2%, and 5.3%. Particularly, for the gene *IGKC*, the correlation coefficient with HisToGene was -0.234, and for the gene *HLA-DRA*, it was -0.058 with STnet.

It is noteworthy that all of the top seven genes identified by mclSTExp are closely linked to breast cancer, playing pivotal roles in its onset and progression. Elevated expression of *GANS* can activate the *PI3K/AKT/Snail1/E-cadherin* pathway, thereby facilitating the proliferation, migration, and invasion of breast cancer cells [32]. *FN1* is recognized as a potential therapeutic target or clinical prognostic marker for breast cancer, as its heightened expression is closely associated with the metastasis and deterioration processes in breast cancer [33]. *FASN* exhibits high expression in cancer stem cells, and its inhibition effectively suppresses the proliferation and survival of breast cancer cells [34]. Moreover, the proliferation,

survival, and aggressiveness of breast cancer cells are closely linked to *SCD*, underscoring its potential as a therapeutic target in breast cancer treatment strategies [35]. Additionally, *IGKC* serves as a prognostic marker with significant value in predicting disease progression and survival outcomes in breast cancer patients [36].

Specifically, among all the compared methods, mclSTExp was the first to predict the genes *HLA-B* and *HLA-DRA*. For one thing, Human leukocyte antigen B (*HLA-B*) belongs to the major histocompatibility complex (MHC) class I molecules, primarily responsible for the presentation of intracellular peptides. A study [37] have indicated that the expression of *HLA-B* is associated with the survival and recurrence rates of breast cancer patients. For another, *HLA-DRA* is a class II MHC molecule typically expressed in professional antigen-presenting cells. Research [38] has demonstrated that *HLA-DRA* serves as a significant prognostic factor for breast cancer. Its expression levels may represent a pathway to enhance the treatment of advanced breast cancer and improve overall survival rates. Another study [39] has highlighted how cancer cells exploit various immune system functions to promote their growth. In summary, the mclSTExp method not only elucidates cancer-specific overexpressed genes but also identifies immune-related genes, providing valuable insights for cancer therapy.

To assess the robustness of our method, we visualized the top seven genes using the same strategy in both the cSCC dataset and the Alex 10x dataset, as detailed in [Supplementary Table S3 and Figure S1](#). These genes have been previously found to be highly associated with human cutaneous squamous cell carcinoma and breast cancer in prior studies [40, 41].

Additionally, we computed the correlation matrix using the expression data of actual genes. Subsequently, hierarchical clustering was performed on this correlation matrix to obtain the clustering order of the samples. Next, we calculated the gene-gene correlations using predicted expression values obtained from various methods, reordered the correlation matrix according to the clustering order, and generated

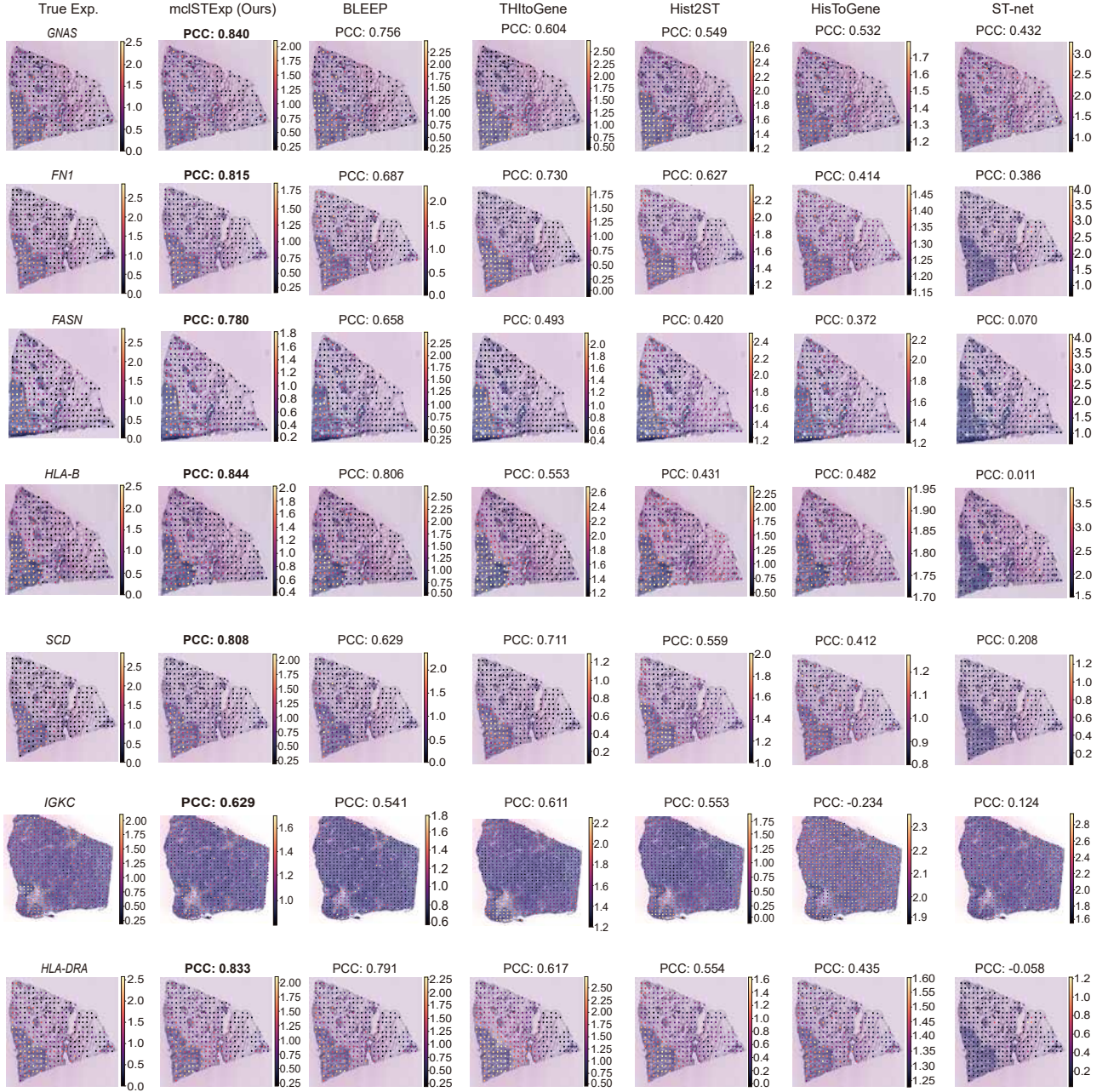


Figure 5. Visualize the top seven predicted genes in the HER2+ dataset based on the highest average $-\log_{10}$ (P-values) calculated across all tissue sections. The P-values are determined based on the correlation between predicted and observed gene expressions. For each of these seven genes, select the tissue section predicted by our model with the smallest P-value for visualization.

a heatmap of the correlations (Supplementary Figure S2). The results indicate that mclSTExp effectively preserves the patterns of gene-gene co-expression and biological heterogeneity.

Spatial region detection

To evaluate the performance of various methods in identifying specific spatial domains on entire H&E images, we compared six tissue slices from the HER2+ dataset. These slices have been annotated by pathologists for spatial transcriptomic analysis. Initially, we employed PCA dimensionality reduction

on the predicted data from mclSTExp, followed by K-Means clustering, as detailed in Supplementary Note 6 and Figure S3.

Ablation studies

To further investigate the contributions of each component of mclSTExp, we conducted a series of ablation experiments on the HER2+, cSCC, and Alex+10x datasets (Supplementary Note 7, Figure S4, Tables S4, S5 and S6).

Discussion and Conclusion

In this study, we propose mclSTExp, a multimodal deep learning approach utilizing Transformer and contrastive learning framework for predicting gene expression from H&E images (Figure 1). Inspired by the field of natural language processing, we regard the spots detected by ST technology as “words” and the sequences of these spots as “sentences” containing multiple “words”. We employ a self-attention mechanism to extract features from these “words” and combine them with learnable position encoding to seamlessly integrate the positional information of these “words”. Subsequently, we adopt a contrastive learning approach, maximizing the cosine similarity of positive samples to bring the correctly matched image blocks and “words” pair samples closer, while minimizing the cosine similarity of negative samples to push away incorrectly matched samples, thereby integrating image information. Through this approach, we learn a multimodal embedding space. Finally, we select the features of the top k “words” with the highest cosine similarity, and then aggregate their true expression spectra by weight to infer the gene expression of the test data.

mclSTExp enables us to predict gene expression from H&E images more accurately. Based on our experimental results, the PCC (ACG) of mclSTExp was 23.01%, 32.09%, and 25.56% higher than that of the second-ranked method BLEEP on the HER2+ dataset, cSCC dataset, and Alex+10x dataset, respectively. Similarly, the PCC (HEG) was 32.89%, 36.48%, and 27.82% higher, respectively. Additionally, mclSTExp exhibits the capability to interpret cancer-specific overexpressed genes and identify specific spatial domains annotated by pathologists.

References

1. Anjali Rao, Dalia Barkley, Gustavo S França, and Itai Yanai. Exploring tissue architecture using spatial transcriptomics. *Nature*, 596(7871):211–220, 2021.
2. Shahr Alon, Daniel R Goodwin, Anubhav Sinha, Asmamaw T Wassie, Fei Chen, Evan R Daugharthy, Yosuke Bando, Atsushi Kajita, Andrew G Xue, Karl Marrett, et al. Expansion sequencing: Spatially precise in situ transcriptomics in intact biological systems. *Science*, 371(6528):2656–2669, 2021.
3. Ao Chen, Sha Liao, Mengnan Cheng, Kailong Ma, Liang Wu, Yiwei Lai, Xiaojie Qiu, Jin Yang, Jiangshan Xu, Shijie Hao, et al. Spatiotemporal transcriptomic atlas of mouse organogenesis using dna nanoball-patterned arrays. *Cell*, 185(10):1777–1792, 2022.
4. Sophia K Longo, Margaret G Guo, Andrew L Ji, and Paul A Khavari. Integrating single-cell and spatial transcriptomics to elucidate intercellular tissue dynamics. *Nature Reviews Genetics*, 22(10):627–644, 2021.
5. Edward Zhao, Matthew R Stone, Xing Ren, et al. Spatial transcriptomics at subspot resolution with bayesspace. *Nature Biotechnology*, 39(11):1375–1384, 2021.
6. Hang Xu, Huazhu Fu, Yahui Long, Kok Siong Ang, Raman Sethi, Kelvin Chong, Mengwei Li, Rom Uddamvathanak, Hong Kai Lee, Jingjing Ling, et al. Unsupervised spatially embedded deep representation of spatial transcriptomics. *Genome Medicine*, 16(1):12–27, 2024.
7. Kangning Dong and Shihua Zhang. Deciphering spatial domains from spatially resolved transcriptomics with an adaptive graph attention auto-encoder. *Nature Communications*, 13(1):1739–1750, 2022.
8. Jiachen Li, Siheng Chen, Xiaoyong Pan, Ye Yuan, and Hong-Bin Shen. Cell clustering for spatial transcriptomics data with graph neural networks. *Nature Computational Science*, 2(6):399–408, 2022.
9. Wenwen Min, Donghai Fang, Jinyu Chen, and Shihua Zhang. Dimensionality reduction and denoising of spatial transcriptomics data using dual-channel masked graph autoencoder. *bioRxiv*, pages 1–20, 2024.
10. Daiwei Zhang, Amelia Schroeder, Hanying Yan, Haochen Yang, Jian Hu, Michelle YY Lee, Kyung S Cho, Katalin Susztak, George X Xu, Michael D Feldman, et al. Inferring super-resolution tissue architecture by integrating spatial transcriptomics with histology. *Nature Biotechnology*, pages 1–9, 2024.
11. Jian Hu, Kyle Coleman, Daiwei Zhang, Edward B Lee, Humam Kadara, Linghua Wang, and Mingyao Li. Deciphering tumor ecosystems at super resolution from spatial transcriptomics with tesla. *Cell Systems*, 14(5):404–417, 2023.
12. Xiaoyu Li, Wenwen Min, Shunfang Wang, Changmiao Wang, and Taosheng Xu. stmcdi: Masked conditional diffusion model with graph neural network for spatial transcriptomics data imputation. *arXiv preprint arXiv:2403.10863*, 2024.
13. Lisa N Waylen, Hieu T Nim, Luciano G Martelotto, and Mirana Ramialison. From whole-mount to single-cell spatial assessment of gene expression in 3d. *Communications Biology*, 3(1):602–613, 2020.
14. Nicola Crosetto, Magda Bienko, and Alexander Van Oudenaarden. Spatially resolved transcriptomics and beyond. *Nature Reviews Genetics*, 16(1):57–66, 2015.
15. Andreas E Moor and Shalev Itzkovitz. Spatial transcriptomics: paving the way for tissue-level systems biology. *Current Opinion in Biotechnology*, 46:126–133, 2017.
16. Minxing Pang, Kenong Su, and Mingyao Li. Leveraging information in spatial transcriptomics to predict super-resolution gene expression from histology images in tumors. *BioRxiv*, pages 1–31, 2021.
17. Shmatko A, Ghaffari Laleh N, Gerstung M, and Kather JN. Artificial intelligence in histopathology: enhancing cancer research and clinical oncology. *Nature Cancer*, 3(9):1026–1038, 2022.
18. Benoît Schmauch, Alberto Romagnoni, Elodie Pronier, Charlie Saillard, Pascale Maillé, Julien Calderaro, Aurélie Kamoun, Meriem Sefta, Sylvain Toldo, Mikhail Zaslavskiy, et al. A deep learning model to predict rna-seq expression of tumours from whole slide images. *Nature Communications*, 11(1):3877–3892, 2020.
19. Richard J Chen, Ming Y Lu, Jingwen Wang, et al. Pathomic fusion: an integrated framework for fusing histopathology and genomic features for cancer diagnosis and prognosis. *IEEE Transactions on Medical Imaging*, 41(4):757–770, 2020.
20. Viktor Petukhov, Rosalind J Xu, Ruslan A Soldatov, Paolo Cadinu, Konstantin Khodosevich, Jeffrey R Moffitt, and Peter V Kharchenko. Cell segmentation in imaging-based spatial transcriptomics. *Nature Biotechnology*, 40(3):345–354, 2022.
21. Chongyue Zhao, Zhongli Xu, Xinjun Wang, Shiyue Tao, William A MacDonald, Kun He, Amanda C Poholek, Kong Chen, Heng Huang, and Wei Chen. Innovative super-resolution in spatial transcriptomics: a transformer model

- exploiting histology images and spatial gene expression. *Briefings in Bioinformatics*, 25(2):1–15, 2024.
22. Bryan He, Ludvig Bergenstr hle, Linnea Stenbeck, Abubakar Abid, Alma Andersson,  ke Borg, Jonas Maaskola, Joakim Lundeb rg, and James Zou. Integrating spatial gene expression and breast tumour morphology via deep learning. *Nature Biomedical Engineering*, 4(8):827–834, 2020.
 23. Yuansong Zeng, Zhuoyi Wei, Weijiang Yu, Rui Yin, Yuchen Yuan, Bingling Li, Zhonghui Tang, Yutong Lu, and Yuedong Yang. Spatial transcriptomics prediction from histology jointly through transformer and graph neural networks. *Briefings in Bioinformatics*, 23(5):297–309, 2022.
 24. Yuran Jia, Junliang Liu, Li Chen, Tianyi Zhao, and Yadong Wang. THItGene: a deep learning method for predicting spatial transcriptomics from histological images. *Briefings in Bioinformatics*, 25(1):464–474, 2024.
 25. Ronald Xie, Kuan Pang, et al. Spatially resolved gene expression prediction from histology images via bi-modal contrastive learning. In *Advances in Neural Information Processing Systems*, pages 1–12, 2024.
 26. Gao Huang, Zhuang Liu, Laurens Van Der Maaten, and Kilian Q Weinberger. Densely connected convolutional networks. In *IEEE Conference on Computer Vision and Pattern Recognition*, pages 4700–4708, 2017.
 27. Alexey Dosovitskiy, Lucas Beyer, Alexander Kolesnikov, Dirk Weissenborn, Xiaohua Zhai, Thomas Unterthiner, Mostafa Dehghani, Matthias Minderer, Georg Heigold, Sylvain Gelly, Jakob Uszkoreit, and Neil Houlsby. An image is worth 16x16 words: Transformers for image recognition at scale. In *International Conference on Learning Representations*, pages 1–22, 2021.
 28. Keyulu Xu, Chengtao Li, Yonglong Tian, Tomohiro Sonobe, Ken-ichi Kawarabayashi, and Stefanie Jegelka. Representation learning on graphs with jumping knowledge networks. In *International Conference on Machine Learning*, pages 5453–5462. PMLR, 2018.
 29. Ting Chen, Simon Kornblith, Mohammad Norouzi, and Geoffrey Hinton. A simple framework for contrastive learning of visual representations. In *International Conference on Machine Learning*, pages 1597–1607. PMLR, 2020.
 30. Kaiming He, Xiangyu Zhang, Shaoqing Ren, and Jian Sun. Deep residual learning for image recognition. In *IEEE Conference on Computer Vision and Pattern Recognition*, pages 770–778, 2016.
 31. Alec Radford, Jong Wook Kim, Chris Hallacy, Aditya Ramesh, Gabriel Goh, Sandhini Agarwal, Girish Sastry, Amanda Askell, Pamela Mishkin, Jack Clark, et al. Learning transferable visual models from natural language supervision. In *International Conference on Machine Learning*, pages 8748–8763. PMLR, 2021.
 32. X Jin, L Zhu, Z Cui, J Tang, M Xie, and G Ren. Elevated expression of gnas promotes breast cancer cell proliferation and migration via the pi3k/akt/snail1/e-cadherin axis. *Clinical and Translational Oncology*, 21:1207–1219, 2019.
 33. Yanxia Wang, Hui Xu, Baoan Zhu, Zhenling Qiu, and Zaijun Lin. Systematic identification of the key candidate genes in breast cancer stroma. *Cellular and Molecular Biology Letters*, 23:1–15, 2018.
 34. Javier A Menendez and Ruth Lupu. Fatty acid synthase (fasn) as a therapeutic target in breast cancer. *Expert Opinion on Therapeutic Targets*, 21(11):1001–1016, 2017.
 35. Ashley M Holder, Ana M Gonzalez-Angulo, et al. High stearoyl-coa desaturase 1 expression is associated with shorter survival in breast cancer patients. *Breast Cancer Research and Treatment*, 137:319–327, 2013.
 36. Marcus Schmidt, Karolina Edlund, Jan G Hengstler, Anne-Sophie Heimes, Katrin Almstedt, Antje Lebrecht, Slavomir Krajnak, Marco J Battista, Walburgis Brenner, Annette Hasenburg, et al. Prognostic impact of immunoglobulin kappa c (igkc) in early breast cancer. *Cancers*, 13(14):3626–3639, 2021.
 37. Mar  a Del Mar Noblejas-L  pez et al. Expression of mhc class i, hla-a and hla-b identifies immune-activated breast tumors with favorable outcome. *Oncoimmunology*, 8(10):1–8, 2019.
 38. Diana P Saraiva, Sofia Azeredo-Lopes, Ant  nio, et al. Expression of hla-dr in cytotoxic t lymphocytes: A validated predictive biomarker and a potential therapeutic strategy in breast cancer. *Cancers*, 13(15):3841–3857, 2021.
 39. Timothy D Martin, Rupesh S Patel, et al. The adaptive immune system is a major driver of selection for tumor suppressor gene inactivation. *Science*, 373(6561):1327–1335, 2021.
 40. Chantip Dang, Marc Gottschling, Kizzie Manning, Eoin O’Curra  n, Sylke Schneider, Wolfram Sterry, Eggert Stockfleth, and Ingo Nindl. Identification of dysregulated genes in cutaneous squamous cell carcinoma. *Oncology Reports*, 16(3):513–519, 2006.
 41. Wei Wei, Yan Chen, Jie Xu, Yu Zhou, Xinp  ng Bai, Ming Yang, and Ju Zhu. Identification of biomarker for cutaneous squamous cell carcinoma using microarray data analysis. *Journal of Cancer*, 9(2):400–407, 2018.